







## Denitrification is the major nitrous acid production pathway in boreal agricultural soils

Hem Raj Bhattarai<sup>1,2,7</sup><sup>✉</sup>, Wolfgang Wanek<sup>3,7</sup>, Henri M. P. Siljanen<sup>1</sup>, Jussi G. Ronkainen<sup>1</sup>, Maarit Liimatainen<sup>1,4,5</sup>, Yuntao Hu<sup>3,6</sup>, Hannu Nykänen<sup>1</sup>, Christina Biasi<sup>1</sup> & Marja Maljanen<sup>1</sup>

Nitrous acid (HONO) photolysis produces hydroxyl radicals—a key atmospheric oxidant. Soils are strong HONO emitters, yet HONO production pathways in soils and their relative contributions are poorly constrained. Here, we conduct <sup>15</sup>N tracer experiments and isotope pool dilution assays on two types of agricultural soils in Finland to determine HONO emission fluxes and pathways. We show that microbial processes are more important than abiotic processes for HONO emissions. Microbial nitrate reduction (denitrification) considerably exceeded ammonium oxidation as a source of nitrite—a central nitrogen pool connected with HONO emissions. Denitrification contributed 97% and 62% of total HONO fluxes in low and high organic matter soil, respectively. Microbial ammonium oxidation only produced HONO in high organic matter soil (10%). Our findings indicate that microbial nitrate reduction is an important HONO production pathway in aerobic soils, suggesting that terrestrial ecosystems favouring it could be HONO emission hotspots, thereby influencing atmospheric chemistry.

<sup>1</sup>Department of Environmental and Biological Sciences, University of Eastern Finland, Kuopio, Finland. <sup>2</sup>Natural Resources Institute Finland, Production systems, Milk Production Unit, Maaninka, Finland. <sup>3</sup>Department of Microbiology and Ecosystem Science, Center of Microbiology and Environmental Systems Science, University of Vienna, Vienna, Austria. <sup>4</sup>Water, Energy and Environmental Engineering Research Unit, University of Oulu, Oulu, Finland. <sup>5</sup>Natural Resources Institute Finland, Production systems, Oulu, Finland. <sup>6</sup>Lawrence Berkeley National Laboratory (LBNL), Berkeley, CA, USA. <sup>7</sup>These authors contributed equally: Hem Raj Bhattarai, Wolfgang Wanek. ✉email: [hemraj.bhattarai@luke.fi](mailto:hemraj.bhattarai@luke.fi)

Up to 60% of primary production of atmospheric hydroxyl (OH) radicals can be attributed to photolysis of nitrous acid (HONO)<sup>1</sup>. Hydroxyl radicals are vital for the removal of pollutants and reactive gases, such as carbon monoxide and methane<sup>2,3</sup> from the atmosphere, and they are also an essential precursor of cloud formation by transforming volatile organic compounds into secondary organic aerosols<sup>4,5</sup>. The current global HONO budget is not balanced when all known sources and sinks are included, which suggests that there is a missing source of HONO<sup>6–8</sup>. Although soils have only recently been identified as important HONO emitters<sup>9–17</sup>, soils have been proposed as a key component of this missing HONO source. Soil nitrite ( $\text{NO}_2^-$ ) may be the key HONO precursor<sup>9</sup> but this has not yet been directly demonstrated using <sup>15</sup>N tracer approaches and accounting for primary microbial pathways producing it. Nitrite is mainly produced during microbial ammonia ( $\text{NH}_3$ ) oxidation (autotrophic and heterotrophic nitrification) and nitrate ( $\text{NO}_3^-$ ) reduction (denitrification and dissimilatory nitrate reduction to ammonium (DNRA)) pathways<sup>18–20</sup>. In addition, direct release of HONO by  $\text{NH}_3$  oxidizers (autotrophic nitrifiers) has also been demonstrated<sup>10,21</sup>. Although the mechanisms that underpin HONO production are not yet fully understood, several studies have demonstrated the importance of microbial pathways in soil HONO production<sup>9–17</sup>. However, abiotic pathways (e.g., hydroxylamine+water = HONO) have been proposed but have not been investigated in soils to date<sup>21</sup>.

The first evidence on a potential link between soil HONO emissions and underlying microbial processes was provided conducting <sup>15</sup>N tracer experiments, showing that nitrifiers outpaced denitrifiers in soil HONO emissions<sup>22</sup>. Another study<sup>23</sup>, proving the concept, also provided evidence on the participation of microbial processes in soil HONO emissions, especially the involvement of  $\text{NH}_3$  oxidizers (nitrifiers) by using <sup>15</sup>N-labeled urea. To date, only one systematic study has addressed the pathways of soil HONO formation using a tracer approach (labeled ammonium (<sup>15</sup> $\text{NH}_4^+$ )), highlighting the sole importance of  $\text{NH}_3$  oxidizers in HONO production and excluding the role of  $\text{NO}_3^-$  reduction in aerobic soils<sup>11</sup>. However, microbial  $\text{NO}_3^-$  reduction is a widespread phenomenon in soils of many ecosystems<sup>24</sup>, with  $\text{NO}_2^-$  produced as an intermediate of the process. Recently, the participation of denitrification processes in water-saturated soils (~100% water-holding capacity (WHC)) was demonstrated for soil HONO formation, suggesting that  $\text{NO}_3^-$  reduction to  $\text{NO}_2^-$  under anoxic conditions could be crucial for soil HONO emissions<sup>25</sup>. Nevertheless, besides water-saturated conditions, soil aggregates can also generate anoxic microsites that can favor microbial  $\text{NO}_3^-$  reduction in water-unsaturated soils, e.g., in agricultural soils<sup>26,27</sup>. In addition, the relative contribution of different microbial pathways to HONO production may vary in soils, as—beyond soil moisture and oxygen saturation—microbial activity is also influenced by soil pH, organic matter (OM) content, soil carbon to nitrogen (C:N) ratio, and temperature<sup>19,28,29</sup>. Thus, HONO production could occur at the microscale level and by contrasting pathways that need to be further investigated. Moreover, the proposed abiotic pathway<sup>21</sup> needs to be addressed in soils. Thus, in order to get a better understanding of the processes that contribute to HONO emissions from soils and their impact on the global HONO budget, the expected link between the soil inorganic N cycle and HONO formation requires further investigation<sup>9,30,31</sup>. Agricultural soils, which cover 50% of the global habitable land area<sup>32,33</sup>, possess a strong potential to release HONO because of enhanced N fertilizer use, which is expected to increase by ~2–4-fold by 2050<sup>34</sup>. Therefore, it is crucial to understand HONO production pathways in agricultural ecosystems.

This study focused on the understanding of HONO production and emissions from agricultural soils of the boreal region, which are typically acidic (pH < 7)<sup>9</sup>. To date, only three studies<sup>12,13,15</sup>

have investigated HONO emissions from boreal agricultural soils. Yet, the processes and pathways behind those HONO emissions have not been demonstrated. In this study, we performed a series of <sup>15</sup>N tracer experiments to understand HONO production pathways in two distinct boreal agricultural soils in Finland; one with a low organic matter (LOM) content and the other with a high organic matter (HOM) content (Supplementary Table 1). First, we aimed to distinguish between biotic and abiotic HONO production pathways by adding <sup>15</sup>N-labeled  $\text{NO}_2^-$  (LNi) to both, live, and sterile soils. Second, to determine the contribution of the two main biotic HONO production pathways (microbial  $\text{NH}_3$  oxidation and  $\text{NO}_3^-$  reduction), we performed separate experiments using <sup>15</sup>N-labeled ammonium ( $\text{NH}_4^+$ , LA) and  $\text{NO}_3^-$  (LNa) in live (non-sterilized) soils. The HONO flux rates were then compared with data compiled in a global HONO flux rate synthesis, which was generated for the first time here. In addition, gross  $\text{NO}_2^-$  production rates across soil pH levels, and the contribution of nitrification and denitrification to the soil  $\text{NO}_2^-$  pool were also compared with published data.

## Results

**Time kinetics of added <sup>15</sup> $\text{NO}_2^-$  and  $\text{HO}^{15}\text{NO}$  production in live and sterile soils.** We sterilized the soil samples by autoclaving to ensure that the biotic pathways that produce HONO via  $\text{NO}_2^-$  or  $\text{NH}_3$ -oxidizing microbes were completely blocked. Autoclaving is the most effective sterilization method in soils, though autoclaving can alter the structure of OM content and cause disaggregation, for example, increasing the availability of dissolved organic matter<sup>35</sup>. We examined the <sup>15</sup>N atom percent excess (APE) of emitted HONO ( $\text{HO}^{15}\text{NO}$  APE) and of soil  $\text{NO}_2^-$  (<sup>15</sup> $\text{NO}_2^-$  APE) in live and sterile soil samples from time zero to 240 minutes, after the addition of labeled <sup>15</sup> $\text{NO}_2^-$  (LNi) and unlabeled  $\text{NO}_2^-$  (control) (Fig. 1).

In the LNi treatment under live conditions, labeled <sup>15</sup> $\text{NO}_2^-$  gradually declined (Fig. 1a, b), indicating the presence of active microbial pathways that produce and consume  $\text{NO}_2^-$ . Further, <sup>15</sup> $\text{NO}_2^-$  consumption was not equally accompanied by <sup>15</sup> $\text{NO}_3^-$  production (by nitrifiers) under live conditions (Supplementary Figure 1). Microbial  $\text{NO}_2^-$  production pathways led to a 50% decrease in <sup>15</sup> $\text{NO}_2^-$  APE by the end of the experiments in both soils (Fig. 1a, b, Supplementary Table 2–3). Both soils also showed a steady decrease in  $\text{HO}^{15}\text{NO}$  APE under live conditions, with the HOM soils exhibiting a stronger decrease than the LOM soils. Under sterile conditions, <sup>15</sup> $\text{NO}_2^-$  APE remained stable at the approximate initial values during the whole incubation period, confirming the blockage of biotic pathways that produce  $\text{NO}_2^-$  (Fig. 1c, d). Despite stable <sup>15</sup> $\text{NO}_2^-$  APE,  $\text{HO}^{15}\text{NO}$  APE decreased towards the end of the incubation period under sterile conditions (Fig. 1c, d), although the <sup>15</sup>N depletion of  $\text{HO}^{15}\text{NO}$  occurred later in time and was less pronounced (at least for LOM) than under live conditions.

## Relationship between biotic pathways and HONO production.

To further disentangle the biotic HONO production pathways (in addition to <sup>15</sup> $\text{NO}_2^-$  (LNi; see experiment above)), we added <sup>15</sup> $\text{NH}_4^+$  (LA) and <sup>15</sup> $\text{NO}_3^-$  (LNa) to the live soil samples and measured the subsequent change in <sup>15</sup> $\text{NO}_2^-$  and emissions of  $\text{HO}^{15}\text{NO}$ . We also quantified gross production and gross consumption rates of  $\text{NH}_4^+$ ,  $\text{NO}_2^-$ , and  $\text{NO}_3^-$  in the live soil samples, based on <sup>15</sup>N pool dilution approaches, to better explain the relationship between the microbial pathways that use <sup>15</sup> $\text{NH}_4^+$  and <sup>15</sup> $\text{NO}_3^-$  to produce HONO. Production (i.e., N mineralization) and consumption rates of  $\text{NH}_4^+$  were relatively low and did not differ between soils. Production (i.e., nitrification) and consumption rates of  $\text{NO}_3^-$  were 6–24 times higher than gross  $\text{NH}_4^+$

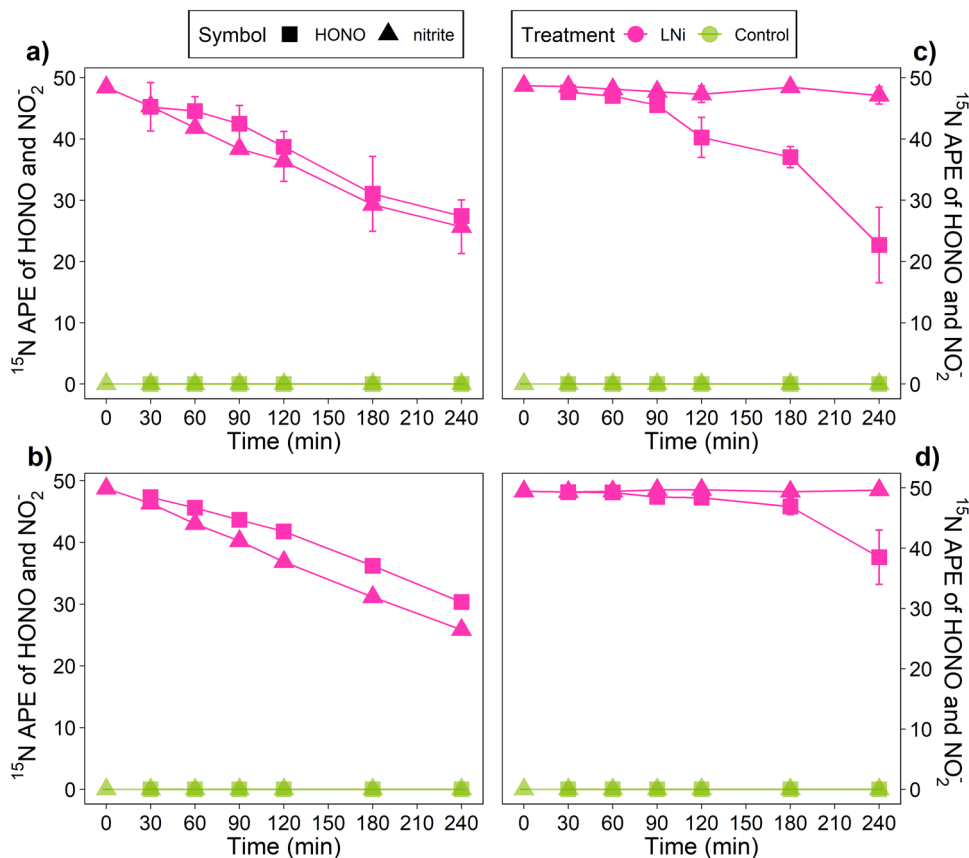


**Fig. 1** The  $^{15}\text{N}$  atom percent excess (APE) of nitrous acid (HONO) and soil nitrite ( $\text{NO}_2^-$ ) in labeled  $^{15}\text{NO}_2^-$  (LNi) and control treatments. The  $^{15}\text{N}$  enriched HONO and  $\text{NO}_2^-$  produced over time (x axis) after the addition of labeled (treatment LNi; pink) or unlabeled  $\text{NO}_2^-$  (treatment control; light green) is shown as  $^{15}\text{N}$  APE of HONO and  $\text{NO}_2^-$  on the y axis. At zero min, labeled  $^{15}\text{NO}_2^-$  was added to increase APE to 50% in the live (a, b) and sterile (c, d) high organic matter soils (a, c) and low organic matter soils (b, d), respectively. The data points show the mean values, and error bars denote standard deviation ( $n = 3$ ). Note: the error bars, in some cases, are smaller than the size of the symbols. Statistical results are shown in Supplementary Tables 2–3.

turnover rates and were significantly higher in the HOM soil than the LOM soil (Fig. 2a). Gross  $\text{NO}_2^-$  production and consumption rates ranged between the values observed for nitrification and mineralization, and were not significantly different between the two studied soils. Production of  $^{15}\text{NO}_2^-$  increased gradually in the LNa treatment in both soils, which exhibited high  $\text{NO}_3^-$  consumption rates (Fig. 2a–c, Supplementary Table 4), indicating that the reduction of  $\text{NO}_3^-$  to  $\text{NO}_2^-$  is a crucial biotic pathway in both water-unsaturated soils. Despite high nitrification rates ( $22 \mu\text{g N g}_{\text{dw}}^{-1} \text{d}^{-1}$ ) in the HOM soil, the magnitude of  $^{15}\text{NO}_2^-$  and  $\text{HO}^{15}\text{NO}$  production during nitrification was smaller compared with  $\text{NO}_3^-$  reduction (Fig. 2b, treatments LA vs. LNa), which suggests that the capability to nitrify by the  $\text{NH}_3$  oxidizers, which reside in the HOM soil, was lower compared with the  $\text{NO}_3^-$  reducers that shared the same environment.

The contribution of the microbial pathways that use  $\text{NH}_4^+$  and  $\text{NO}_3^-$  to total production and emissions of HONO was evident. In general, reduction of  $^{15}\text{NO}_3^-$  affected the production of  $\text{HO}^{15}\text{NO}$  via  $^{15}\text{NO}_2^-$  formation, as  $^{15}\text{N}$  APE values of HONO (on average ~1–18% in the LOM soil and 1.2–18% in the HOM soil) and  $\text{NO}_2^-$  increased gradually with time only in the LNa treatment in both soils (Fig. 2b–c). The strong relationship between produced  $\text{HO}^{15}\text{NO}$  and added  $^{15}\text{NO}_2^-$  (LNi treatment), or with  $^{15}\text{NO}_2^-$  produced from  $^{15}\text{NO}_3^-$  (LNa treatment) (Supplementary Figure 2), further confirmed that HONO was generated mostly from  $\text{NO}_2^-$  produced via microbial  $\text{NO}_3^-$  reduction in both soils. In addition, the observation that HONO emission rates decreased with

decreasing  $\text{NO}_2^-$  concentrations (Supplementary Figures 3–6 and Supplementary Table 4) would also suggest that HONO production and emissions are directly linked to soil  $\text{NO}_2^-$ , especially in LOM soil. The HOM soil showed a curvilinear relationship between HONO emissions and soil  $\text{NO}_2^-$  concentrations (Supplementary Figure 6a), indicating rapid  $\text{NO}_2^-$  consumption processes that competed tightly with HONO production via the soil  $\text{NO}_2^-$  pool. In contrast, microbial  $\text{NH}_4^+$  oxidation occurred only in the HOM soil but not in the LOM soil. Production of  $\text{HO}^{15}\text{NO}$  (from  $0.1 \pm 0.1$  at 30 min to  $0.4 \pm 0.1\%$   $^{15}\text{N}$  APE at 240 min) and  $^{15}\text{NO}_2^-$  (from  $0.2 \pm 0.3$  at 90 min to  $1.6 \pm 1.3\%$   $^{15}\text{N}$  APE at 240 min) from  $^{15}\text{NH}_4^+$  (LA treatment) was less than  $\text{NO}_3^-$  reduction (LNa treatment), and showed a weak, insignificant association (Supplementary Figure 2).

**Quantification of HONO emissions by biotic and abiotic processes.** In the presence of microbial activity in the live soil samples, a two-source isotope mixing model<sup>36</sup> showed that  $\text{NO}_2^-$  contributed 100% to HONO production in the LOM soil and 81% in the HOM soil. In the latter, (in addition to  $\text{NO}_2^-$ ) an additional biotic HONO source contributed 19% to HONO production towards the end of the incubation period (Fig. 3a). Despite the presence of a consistent HONO precursor (i.e.,  $\text{NO}_2^-$ ), the dynamics of biotic HONO emissions in the LOM soil differed from the HOM soil (Fig. 3b). Biotic HONO emissions in the LOM soil peaked at 180 min and then decreased slightly until the end of the incubation, whereas biotic HONO emissions increased

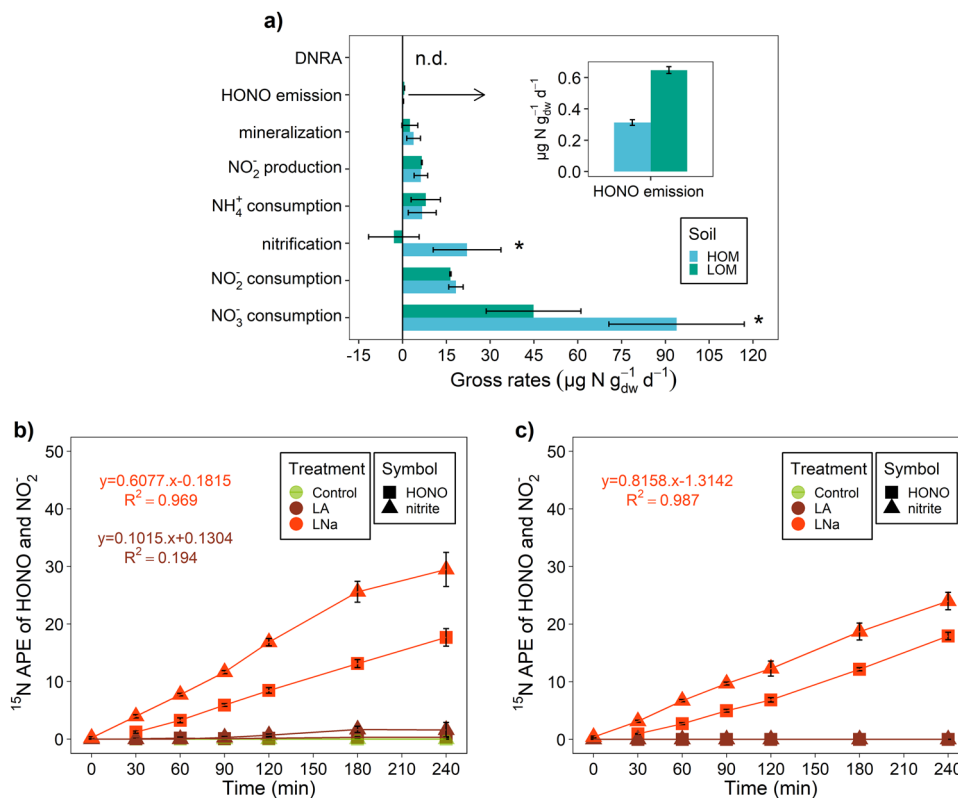


**Fig. 2** Gross transformation rates of mineral nitrogen and production of  $^{15}\text{NO}_2^-$  and  $\text{HO}^{15}\text{NO}$  in live soils. Gross consumption and production rates ( $\mu\text{g N g}_{\text{dw}}^{-1} \text{d}^{-1}$ ) of  $\text{NO}_2^-$ ,  $\text{NO}_3^-$ , and  $\text{NH}_4^+$  in the live soil samples from the high (HOM; sky blue bar) and low (LOM; turquoise bar) organic matter soils are shown on the x axis of **a**. **a** also shows the maximum biotic HONO emission rates expressed in the same units as gross nitrogen transformation rates. For clarity, it is shown as an inset figure.  $^{15}\text{N}$  enriched HONO (squares) and  $\text{NO}_2^-$  (triangles) production over time (x axis) after the addition of  $^{15}\text{NH}_4^+$  (treatment LA; dark brown),  $^{15}\text{NO}_3^-$  (treatment LNa; dark orange), and natural  $^{15}\text{N}$  abundance (treatment control; light green) in the live soil samples from the HOM (**b**) and LOM (**c**) soils are shown as  $^{15}\text{N}$  atom percent excess (APE) of HONO and  $\text{NO}_2^-$  on the y axis. Bars and data points in **a–c** show the mean values, and error bars denote standard deviation ( $n = 3$ ). Nitrification ( $F = 9.00$ ,  $P = 0.03$ ) and  $\text{NO}_3^-$  consumption ( $F = 8.98$ ,  $P = 0.04$ ) rates were significantly higher in the HOM soil than in the LOM soil, which is shown by asterisks. The absence of an asterisk right to the bars in **a** indicates no statistical difference in corresponding rates between the soils. Statistical results for **b** and **c** are shown in Supplementary Tables 2–3. **a** n.d. denotes not detected.

gradually in the HOM soil, and saturated after 180 min (Fig. 1, Fig. 3b). Microbial processes produced  $10.5 \text{ ng N m}^{-2} \text{ s}^{-1}$  and  $24.3 \text{ ng N m}^{-2} \text{ s}^{-1}$  of HONO in the HOM and LOM soils, respectively (Fig. 4).

Although  $^{15}\text{N}$  enrichment of  $\text{NO}_2^-$  remained constant in the sterile soil samples (as expected if only biotic processes form  $\text{NO}_2^-$ ),  $\text{HO}^{15}\text{NO}$  declined, which indicates the presence of an unknown abiotic HONO source (Fig. 3c, d). In the absence of microbial activities in the sterile soils, the unknown HONO production source increased with time (Fig. 3c). Furthermore, the unknown HONO source was more pronounced in the HOM soil than in the LOM soil (Fig. 3c). In the latter, the contribution of the unknown source to total HONO flux peaked at the end of the incubation, reaching a maximum of 22%. In the HOM soil, the contribution from the unknown source increased gradually, exceeding HONO production from soil  $\text{NO}_2^-$  at the end of the incubation, and contributed up to 52%. In both soils, the fractional contributions of the unknown source and abiotic HONO emissions showed similar increasing trends (Fig. 3c, d). In comparison with the LOM soil, the HOM soil had a greater contribution of an unknown source and also greater abiotic HONO emission rates (Fig. 3d).

## Discussion

Soil HONO emissions in our boreal agricultural soils ( $10.5\text{--}24.3 \text{ ng N m}^{-2} \text{ s}^{-1}$ , Fig. 4) were relatively high compared to a global synthesis of soil HONO emission rates (median

$5.0 \text{ ng N m}^{-2} \text{ s}^{-1}$ ,  $n = 199$ ; Fig. 5, Supplementary Data 1), but were reflective of managed soils, where fertilization or grazing promote N cycling, which increases soil HONO emissions (cropland  $\geq$  grassland  $\geq$  forest, and peatland, Fig. 5). Only deserts showed greater HONO emissions, indicating arid biological soil crusts being hotspots of HONO emissions globally<sup>37</sup>.

## Biotic pathways of soil HONO formation and significance.

A consistent decrease in the  $^{15}\text{N}$  enrichment of HONO, in parallel with that in  $\text{NO}_2^-$  in the live soil samples, and much higher rates of HONO production in the live soil samples compared with the sterile soil samples confirmed that microbial processes are the most important HONO sources in soils. Although soil HONO emissions have been previously linked to soil  $\text{NO}_2^-$  based on physicochemical reasoning (acid-base equilibria between  $\text{H}^+$  and  $\text{NO}_2^-$ -producing HONO)<sup>9</sup>, here for the first time we unequivocally and causally link the soil  $\text{NO}_2^-$  pool with HONO emissions, based on  $^{15}\text{N}$  tracing and liquid chromatography-high resolution mass spectrometry. The findings further demonstrate that microbial  $\text{NO}_3^-$  reduction dominated HONO production and by far exceeded the concurrently accepted major HONO production pathway, i.e.,  $\text{NH}_3$  oxidation by autotrophic nitrifiers, in aerobic, water-unsaturated soils, here boreal agricultural soils (Figs. 2a–c, 3b). Among the three soil  $\text{NO}_2^-$ -producing microbial pathways, only  $\text{NO}_3^-$  reduction triggered significant  $^{15}\text{NO}_2^-$  and  $\text{HO}^{15}\text{NO}$  production in both soils. Soil  $\text{NO}_3^-$  reduction was

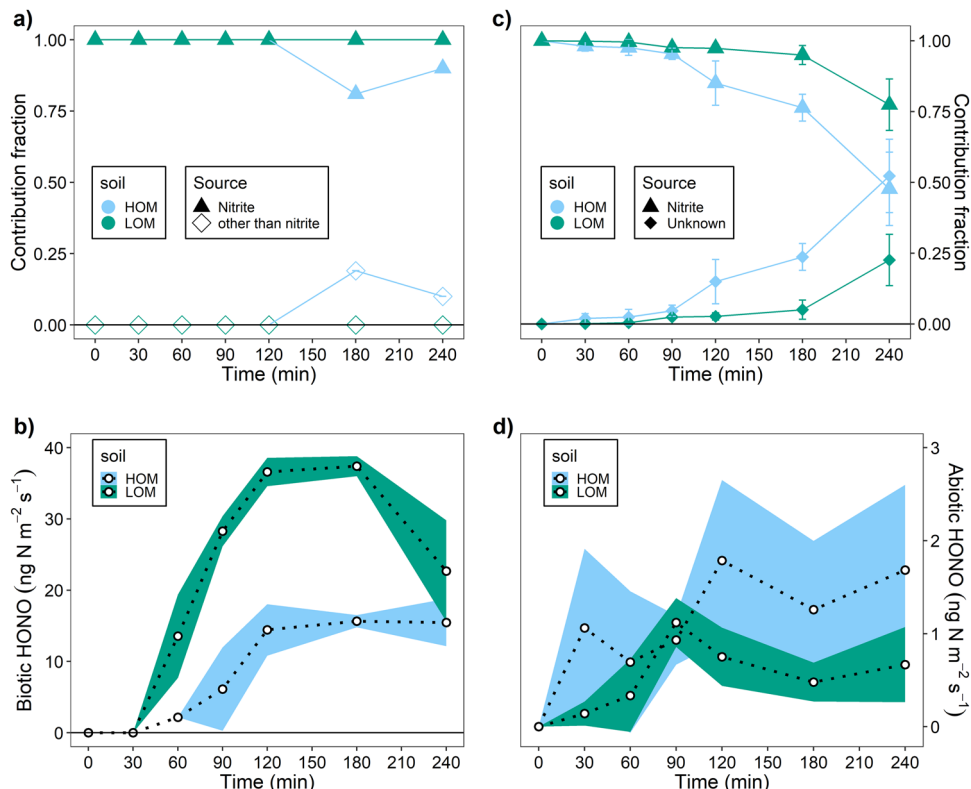


**Fig. 3** Source contribution and nitrous acid (HONO) emission rates from biotic and abiotic sources. **a, c** Show the fraction of source contributions in live and sterile soil samples, respectively, from the high organic matter (HOM; sky blue) and low organic matter (LOM; turquoise) soils. **b, d** Show the biotic and abiotic HONO emission rates (ng N m<sup>-2</sup> s<sup>-1</sup>), respectively, in both soils. The symbols in **a** and **c** indicate the HONO sources, nitrite (NO<sub>2</sub><sup>-</sup>; triangles), sources other than NO<sub>2</sub><sup>-</sup> (empty diamonds), and unknown (filled diamonds). Data points with error bars in **a, c** and filled areas in **b** and **d** show the mean values and standard deviation (*n* = 3). Source contributions to soil HONO emissions at 180 and 240 min in **a** are the maximum values from a single replicate in HOM soil. **a-d** were created using the data from the LNi treatment of the respective soils and conditions (see the Methods section for details).

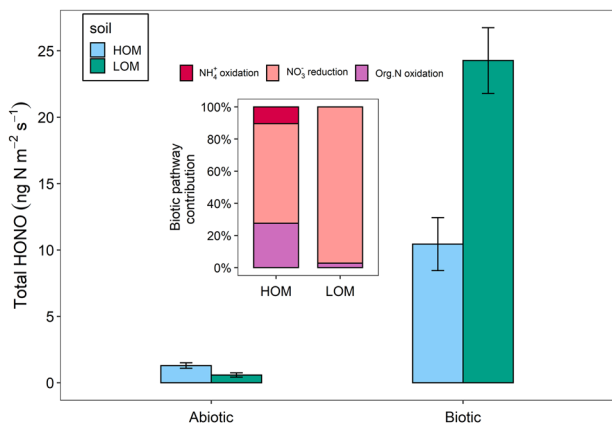


**Fig. 4** Total soil nitrous acid (HONO) emission rates via abiotic and biotic processes, with the relative contribution of biotic pathways to HONO production as inset. Total HONO emissions represent the rate of soil HONO production averaged over 240 minutes of HONO flux measurements. Total HONO production rates (ng N m<sup>-2</sup> s<sup>-1</sup>) for the soils with high organic matter content (HOM, sky blue bar) and low organic matter (LOM, turquoise bar) are shown on the y axis. Bars show the mean values, and the error bars denote the standard deviation (*n* = 3). Inset shows the fractional contribution of microbial ammonium (NH<sub>4</sub><sup>+</sup>) oxidation (dark red), nitrate (NO<sub>3</sub><sup>-</sup>) reduction (light brick red), and organic nitrogen (org. N) oxidation to nitrite (purple) pathways in each soil.

solely linked to the presence of the periplasmic NO<sub>3</sub><sup>-</sup> reductase (*napA*) gene, as the cytoplasmic NO<sub>3</sub><sup>-</sup> reductase (*narG*) gene<sup>38</sup> was absent in both soils (Supplementary Figure 7). The lack of <sup>15</sup>NH<sub>4</sub><sup>+</sup> production from <sup>15</sup>NO<sub>3</sub><sup>-</sup> in the LNa treatment (Supplementary Figure 1) suggests that DNRA (dissimilatory nitrate reduction to ammonium) was absent and that denitrification dominated microbial NO<sub>3</sub><sup>-</sup> reduction and soil HONO emissions. This is further confirmed by the absence of the key DNRA gene, i.e., nitrite reductase (*nrfA*)<sup>18,39</sup>, whereas the genes of key denitrifying genes were abundant, e.g. *napA*, *nirK*, *nirS*, and *nosZ* (Supplementary Figure 7). Nitrification only contributed to a small extent to soil HONO production (Fig. 4), and was only found in the HOM soil (Fig. 2b). Nitrification could be attributed to the presence of bacterial and archaeal NH<sub>3</sub> oxidizers<sup>10,21</sup>, as suggested by higher gene copy numbers of bacterial (and archaeal) ammonia monooxygenase (*amoA*) in the HOM soil (Supplementary Figure 7), and these are capable of directly producing HONO<sup>10</sup> before accumulating NO<sub>2</sub><sup>-</sup> (Supplementary Figure 2). Decoupling of microbial NO<sub>3</sub><sup>-</sup> reduction (high <sup>15</sup>NO<sub>2</sub><sup>-</sup> output, Fig. 2a) and biotic HONO production (Fig. 4) in the HOM soil could be associated with the combined effect of microbial NO<sub>2</sub><sup>-</sup> consumption and abiotic NO<sub>2</sub><sup>-</sup> reactions with soil OM via nitration and nitrosation<sup>40</sup>. In these soils, we observed a curvilinear relationship between soil NO<sub>2</sub><sup>-</sup> concentrations and HONO emission rates (Supplementary Figure 6a), which indicates a gradual conversion of NO<sub>2</sub><sup>-</sup> to NO<sub>3</sub><sup>-</sup> (Supplementary Figure 1) and concurrently occurring chemical reactions between NO<sub>2</sub><sup>-</sup> and soil OM<sup>40</sup>, the latter of which surpass HONO formation via NO<sub>2</sub><sup>-</sup> after reaching an optimum.

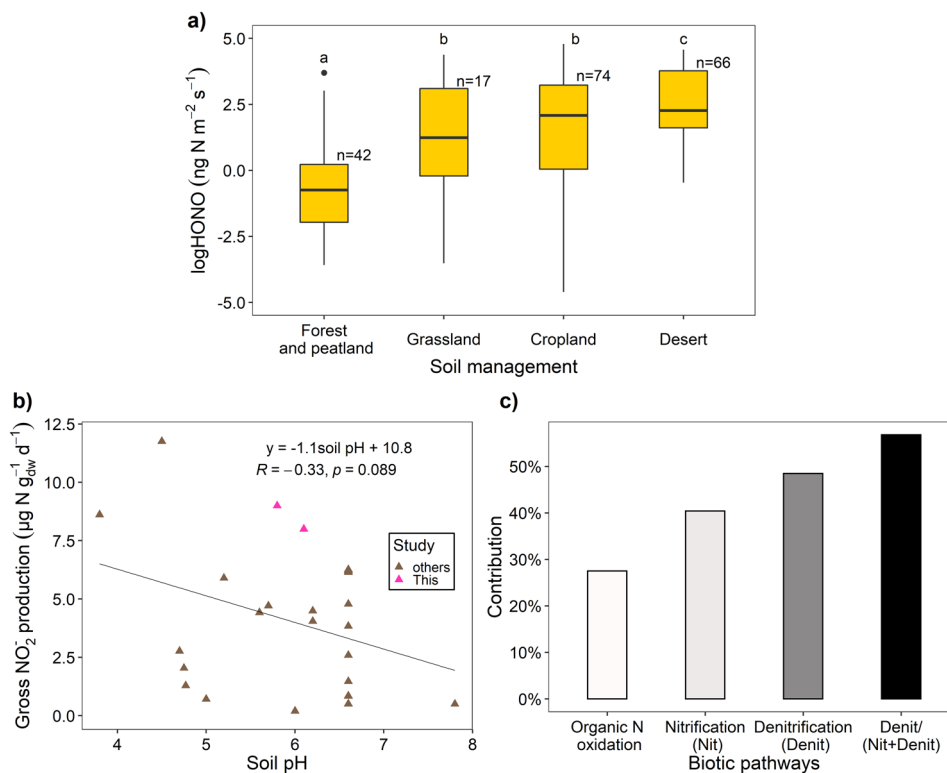


**Fig. 5 Global synthesis of soil nitrous acid (HONO) emissions rates, gross nitrite ( $\text{NO}_2^-$ ) production, and the contribution of biotic pathways to the soil  $\text{NO}_2^-$  pool.** **a** Shows log-transformed HONO emission rates ( $\text{ng N m}^{-2} \text{s}^{-1}$ ) from the soils of a number of ecosystems under different management practices. Each yellow box denotes interquartile range (IQR); 25th percentile at lower end to the 75th percentile at upper end) with a central black line as median, lower whisker as a minimum (25th percentile  $- 1.5 \times \text{IQR}$ ), upper whisker as a maximum (75th percentile  $+ 1.5 \times \text{IQR}$ ), and filled black circle as an outlier of sample numbers presented above the boxes of respective soil management practices. See Supplementary Data 1 for more details. Different letters in **a** indicate significant differences between means ( $F = 22.64$ ,  $P < 0.05$ ) in HONO emissions in different ecosystems. The correlation in **b** shows the relationship between gross nitrite production rates ( $\mu\text{g N g}_{\text{dw}}^{-1} \text{d}^{-1}$ ) and soil pH in this study (pink triangle) and from synthesized data (light brown), i.e., Supplementary Data 2. The slope in **b** is marginally significant ( $P < 0.1$ ), whereas the intercept is significant at  $P < 0.05$ . **c** Shows the percentage (%) contribution of different biotic pathways, organic nitrogen oxidation (white bar), nitrification (light gray bar), denitrification (dark gray bar), and ratio of denitrification to sum of nitrification and denitrification (black bar) to the soil  $\text{NO}_2^-$  pool. See Supplementary Data 2 for more details.

Soil moisture is an important environmental driver of soil HONO emissions. Maximum soil HONO emissions were identified in a wide range of ecosystems under low soil moisture contents (“dry” peak at 20–30% WHC)<sup>9,10,25</sup>. Such HONO emission peaks occurred during progressive reduction in soil moisture in the experiments and were linked to nitrifiers as  $\text{NH}_3$  oxidation is an aerobic pathway and requires oxygen. Therefore, it was assumed that with soil moisture reduction and progressively developing the aerobic condition,  $\text{NH}_3$  oxidation<sup>10,21</sup> dominates soil HONO production and emissions. However, the  $^{15}\text{NH}_4^+$  supplemented LOM soil did not emit  $\text{HO}^{15}\text{NO}$ , even until the end of the experimental period, despite a slight reduction in soil moisture (from 60%<sub>start</sub> to 51%<sub>end</sub> WHC; Supplementary Figure 8). In contrast,  $^{15}\text{NH}_4^+$  supplemented HOM started to emit  $\text{HO}^{15}\text{NO}$ , presumably by  $\text{NH}_3$  oxidizers<sup>10,21</sup>, from the middle of the experiment (Fig. 2b, Supplementary Table 2–3), despite a smaller reduction in soil moisture (from 60%<sub>start</sub> to 54%<sub>end</sub> WHC) compared with the LOM soil (Supplementary Figure 8). In our study, we did not measure HONO emissions for longer periods and therefore did not reach lower soil moisture regimes, for example, 20–30% WHC, at which the contribution of nitrifier pathways could increase<sup>10,21</sup>. For example, Wu et al.<sup>23</sup> showed that soil HONO emissions (at 20–30% WHC) were driven by  $\text{NH}_3$  oxidation in a pH neutral soil from the temperate region. On the other hand, Kubota and Asami<sup>22</sup> estimated that ~69% of the soil emitted HONO originated from  $\text{NH}_3$  oxidation at 60% WHC from

sub-tropical acidic soils (pH = 4.8–5.8) incubated at 30°C for 30 days. Our estimation shows that  $\text{NH}_3$  oxidation contributed only 0–10% to the total biotic HONO emissions (at 60–54% WHC range) from slightly acidic (pH = 6.1) boreal agricultural soils incubated at 21 °C for 48 hours. The likely reason for higher contributions of nitrifiers to soil HONO emissions in the two earlier studies<sup>22,23</sup> could be differences in soil moisture and temperature between studies, which are known to control the activities of  $\text{NH}_3$  oxidizers<sup>29</sup> and thereby of soil HONO emissions<sup>10,23,25</sup>. Nevertheless, our results obtained from the LA treatments in two boreal agricultural soils suggest that the capabilities of  $\text{NH}_3$  oxidizers to produce HONO<sup>10,21</sup> vary according to soil type and/or climatic zone, which requires further studies.

Besides soil moisture, soil pH also has a significant role in HONO emissions. Although nitrification (especially by bacterial ammonia oxidizers) decreases towards low soil pH levels<sup>41</sup>, at the same time, regardless of its source, rapid protonation of  $\text{NO}_2^-$  in acidic soils<sup>9</sup> can promote soil HONO formation and release. The reported HONO release from soils by acidophilic and high  $\text{NH}_3$  affinity archaea<sup>11,41,42</sup> was lower than HONO emissions via microbial  $\text{NO}_3^-$  reduction (Supplementary Figure 9), further supporting our finding that soil  $\text{NO}_2^-$  via microbial  $\text{NO}_3^-$  reduction is crucial for HONO production, especially in soils with pH < 7. In addition, denitrification demands the presence of protons ( $2\text{NO}_3^- + 10\text{e}^- + 12\text{H}^+ \rightarrow \text{N}_2 + 6\text{H}_2\text{O}$ ) and therefore shows a pH optimum under acidic conditions unlike nitrification,

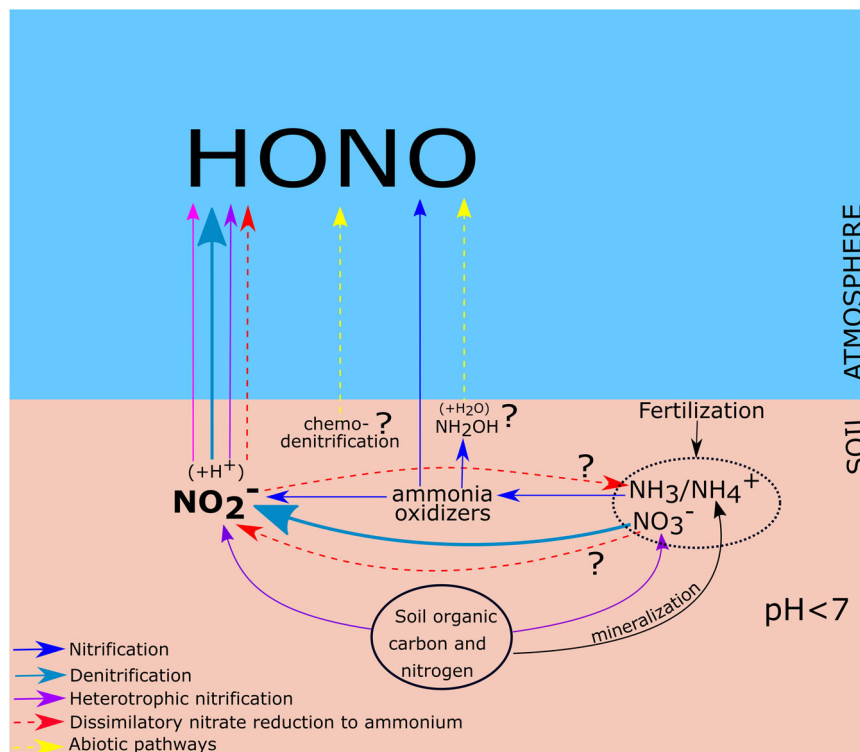


**Fig. 6 Conceptual model showing nitrous acid (HONO) production pathways associated with the nitrogen cycle in agricultural soils.** Pathways associated with HONO production are indicated with solid colored arrows and are defined at the bottom left of the figure. Pathways that are yet to be confirmed (e.g.,  $\text{NH}_2\text{OH} + \text{H}_2\text{O}$  and DNRA) or having potential but were not studied yet, i.e., chemo-denitrification concerning HONO production in soils, are indicated by dotted colored arrows and with question marks (?). Chemo-denitrification is a process associated with the abiotic reaction of nitrite or nitrate in the presence of amines, reduced metals (e.g.,  $\text{Fe}^{2+}$ ), and high soil organic carbon<sup>47–49</sup> to gaseous nitrogen forms. Arrows denoting denitrification are thickest, indicating denitrification to be the most significant pathway of HONO production via the soil nitrite ( $\text{NO}_2^-$ ) pool in soils with  $pH < 7$ . This conceptual model is based on findings here, and literatures published earlier.

which does the opposite, i.e., it releases  $\text{H}^+$  ( $\text{NH}_3 + 2\text{O}_2 \rightarrow \text{NO}_3^- + \text{H}^+ + \text{H}_2\text{O}$ ) into the soil and therefore shows a pH optimum at neutral to alkaline conditions. Therefore, acidic soils are likely to favor  $\text{NO}_3^-$  reduction via denitrification under suitable conditions, such as ample  $\text{NO}_3^-$  availability and anoxic microsites. Moreover, our data synthesis clearly shows that gross  $\text{NO}_2^-$  production rates increase in acidic soils (Fig. 5b, Supplementary Data 2). In published studies that have examined the contribution of nitrifiers and denitrifiers to soil  $\text{NO}_2^-$  production, an average 48% and 57% of the  $\text{NO}_2^-$  source was contributed by denitrifiers ( $n = 82$ , Fig. 5c, Supplementary Data 2), when organic N oxidation to  $\text{NO}_2^-$  by heterotrophic nitrifiers was included or excluded. The relationship between soil  $\text{NO}_3^-$  reduction by denitrifiers and soil HONO emissions as found in our study is in agreement with Wu et al.<sup>25</sup> who recently demonstrated high HONO emissions from soils under water-saturated, anaerobic conditions (“wet” peak caused by microbial  $\text{NO}_3^-$  reduction at ~100% WHC). However, here we show the importance of microbial  $\text{NO}_3^-$  reduction for HONO production under water-unsaturated, aerobic soil conditions (between 51% and 60% WHC). This suggests that not only water-saturated, anoxic soils, but also anoxic microsites in aerobic soils that are commonly generated in the interior of soil aggregates<sup>26</sup> are key to the promotion of microbial  $\text{NO}_3^-$  reduction and soil HONO formation. Therefore, soil HONO production via microbial  $\text{NO}_3^-$  reduction in aggregates is likely a more widespread phenomenon because of the anoxic soil microsites and the ubiquity and diversity of  $\text{NO}_3^-$  reducers (archaea, fungi, bacteria) in a wide range of ecosystems<sup>24,43</sup>, and across a wide range of soil pH and moisture contents.

**Abiotic pathway of soil HONO formation.** Decreasing  $^{15}\text{N}$  enrichment in HONO in sterile soils, despite the constant  $^{15}\text{N}$  enrichment in  $\text{NO}_2^-$ , suggests the presence of an abiotic HONO production pathway. With consistent  $^{15}\text{N}$  enrichment in  $\text{NO}_2^-$  and zero microbial production and consumption of  $\text{NO}_2^-$  (Fig. 1), we can only assign the observed HONO flux to an unknown abiotic source, not related to the soil  $\text{NO}_2^-$  pool. As our HONO measurements were conducted in Teflon coated (inner wall) chambers in the dark, heterogeneous reactions that require nitrogen dioxide ( $\text{NO}_2$ ) and light conditions to form HONO<sup>44,45</sup> are expected to be insignificant. Also, the absence of microbial  $\text{NO}_2^-$  production in sterile conditions precludes the possibility of HONO production via self-decomposing  $\text{HNO}_2$ , as its products ( $\text{NO}_2$  and nitric oxide (NO) gases) must pass through the soil  $\text{NO}_2^-$  pool<sup>46</sup>. Recently, a reaction between soil hydroxylamine and  $\text{H}_2\text{O}$  has been suggested to produce HONO abiotically on glass beads<sup>21</sup>, although there is little evidence for this phenomenon in soils. Nevertheless, abiotic production of HONO was twofold higher (Fig. 4) in the HOM soil ( $1.3 \text{ ng N m}^{-2} \text{ s}^{-1}$ ) compared with the LOM soil ( $0.6 \text{ ng N m}^{-2} \text{ s}^{-1}$ ), which indicates that soil OM may play a role in the abiotic formation of HONO. This unidentified abiotic HONO pathway, which does not require passage through the soil  $\text{NO}_2^-/\text{HNO}_2$  pool, clearly needs further investigation.

## Conclusion

We confirmed that microbial processes are essential for HONO emissions from agricultural soils, as they contributed 8–42 times more to soil HONO emissions than abiotic processes (Fig. 4). Using  $^{15}\text{NO}_2^-$ ,  $^{15}\text{NO}_3^-$ , and  $^{15}\text{NH}_4^+$  tracers, we showed, for the

first time, that microbial  $\text{NO}_3^-$  reduction (denitrifiers) is driving soil HONO emissions in aerobic soils, by fueling the soil  $\text{NO}_2^-$ . Other microbial pathways contributed little or not to HONO production, i.e., nitrification ( $\text{NH}_3$  and organic N oxidation) and DNRA (Figs. 4, 6). We conclude that microbial processes are essential for soil HONO emissions, and that the microbial  $\text{NO}_3^-$  reduction pathway could be a significant contributor in aerobic soils of many ecosystems. Moreover, abiotic HONO production pathways that have remained elusive could exist in soils, thereby contributing to notable emissions of HONO to the atmosphere, although microbial pathways are dominant. Therefore, in order to better understand the impact of soil emitted HONO on the seasonally changing atmospheric HONO budget, atmospheric OH radical production and associated atmospheric chemistry<sup>30,31,50</sup> (at present and in the future under a changing climate), we suggest that future studies should assess the relative contribution of microbial pathways, in tandem with concurrent abiotic processes (Fig. 6), to soil HONO production, by applying appropriate  $^{15}\text{N}$  tracer approaches.

## Methods

**Soil sampling and sample preparation.** Two soils (HOM and LOM) with distinct edaphic properties (Supplementary Table 1) were sampled from two separate agricultural fields maintained by the Natural Resources Institute Finland (LUKE) in eastern Finland, Maaninka (63°09' N, 27°20' E). According to the World Reference Base of soils<sup>51</sup>, the LOM soil is classified as a Dystric Regosol, which covers 2% of the global land surface and the HOM soil is classified as a Histosol, typical of the northern latitudes, and covers 2.5% of the global land area, though 30% in Finland. The sampled bulk soils (0–20 cm soil depth) were immediately transported to the laboratory where the roots and remaining plant parts were removed manually. Then the soils were homogenized, sieved (4 mm), and stored at 4 °C until the start of the experiments.  $^{15}\text{N}$  tracer experiments were conducted with live (non-sterile) and sterile (autoclaved) soil conditions. More details are described in the Supplementary Methods.

**$^{15}\text{N}$  tracer experiments.** In all, 100 g of soil (live or sterilized) were transferred to a sterile petri dish ( $\varnothing$  0.137 m, h = 0.017 m) with a sterilized spatula, and  $^{15}\text{N}$  tracer solution was added evenly to the soil surface with a pipette, immediately prior to the HONO measurements. We used three different tracers,  $^{15}\text{NO}_2^-$ ,  $^{15}\text{NH}_4^+$ , and  $^{15}\text{NO}_3^-$ , thereby establishing three different treatments: labeled nitrite (LNI), labeled ammonium (LA), and labeled nitrate (LNA), respectively. We also established a control treatment, where live and sterile soil samples received all three N forms at natural  $^{15}\text{N}$  abundance. More details are described in the Supplementary Methods.

**HONO flux measurements and flux calculation.** The  $^{15}\text{N}$ -amended samples were immediately transferred inside an opaque dynamic chamber, and HONO concentrations were measured with a Long Path Absorption Photometer instrument (LOPAP)<sup>52</sup>. The HONO flux was measured as described in Bhattarai et al.<sup>15</sup>. More details are provided in the Supplementary Methods.

**Isotope pool dilution assays and determination of isotope ratios.** The Isotope pool dilution (IPD) assays<sup>53</sup> were performed for all three N pools in live and sterile soil samples. For IPD assays, 4 g fresh soil (live or sterile) were weighed into 50 ml sterile polypropylene tubes (CELLSTAR®, Greiner BIO-ONE) and supplemented with 300  $\mu\text{l}$   $^{15}\text{N}$  tracer mix. Here, concentrations and atom% of tracer solutions and the soil moisture content were the same as used in the HONO flux experiments. After tracer addition, the tubes were vortexed for 2 minutes to allow the tracers to mix sufficiently in the soil matrix. The incubations were stopped by extraction with 30 ml cold (4 °C) 1 M KCl at zero, 30, 60, 90, 120, 180, and 240 minutes. The isotope ratios ( $^{15}\text{N}/^{14}\text{N}$ ) in  $\text{NH}_4^+$  and  $\text{NO}_3^-$  were determined using the micro-diffusion method<sup>53</sup> in the soil extracts collected at zero, 90, 180, and 240 during the IPD experiment. More details are provided in the Supplementary Methods.

**Collection and purification of HONO and  $\text{NO}_2^-$  azo dyes.** The collection and purification of HONO and  $\text{NO}_2^-$  azo dyes were performed following Wu et al.<sup>23</sup>, who established a method to analyze  $^{15}\text{N}$  APE in gaseous HONO. In the LOPAP instrument, HONO is reacted to an azo dye ( $\text{C}_{18}\text{H}_{19}\text{O}_2\text{N}_5\text{S}$ ). Gaseous HONO is scrubbed in two sequential reactions, first with acidic sulfanilamide solution ( $\text{R}_1$ ) in a two-channel stripping coil, and second with N-(1-Naphthyl)ethylenediamine solution ( $\text{R}_2$ ), which was collected separately from channel 1 and channel 2 after photometric detection in the LOPAP<sup>52</sup>. Each 5 ml of HONO azo dye solution was collected in 15 ml sterile polypropylene tubes (CELLSTAR®, Greiner BIO-ONE) at six sampling points that ended at 30, 60, 90, 120, 180, and 240 minutes after connecting the soil samples to the LOPAP. In parallel,  $\text{NO}_2^-$  azo dyes were

produced from the soil extracts collected during the IPD experiment and standards using an identical approach for preparing azo dye<sup>23</sup>. Immediately upon extract collection at each time point, 5 ml azo dye was generated by reacting 2.5 ml  $\text{R}_1 + \text{R}_2$  mix (mixed at 1:1 (v:v) ratio) with 2.5 ml soil extract or standards. The  $\text{R}_1$  and  $\text{R}_2$  solutions used in the LOPAP instrument and for generating  $\text{NO}_2^-$  azo dyes in the soil extracts were of the same concentrations and the same chemical brand. The generation of  $\text{NO}_2^-$  azo dye from the soil extracts in the IPD assays was done for the first time in this study to understand the dynamics in the isotope ratios ( $^{15}\text{N}/^{14}\text{N}$ ) of  $\text{NO}_2^-$  produced by different microbial N cycling pathways and to relate them to the isotope dynamics of HONO emitted from soils. HONO and  $\text{NO}_2^-$  azo dyes were purified by a reversed-phase extraction, according to Wu et al.<sup>23</sup>, except for the volume of acetonitrile and milli-Q  $\text{H}_2\text{O}$  used for the pre-conditioning and final washing step of SPE (Solid Phase Extraction) columns. We used 1 ml acetonitrile and 2 ml milli-Q  $\text{H}_2\text{O}$  more than used by Wu et al.<sup>23</sup>, to ensure the best cleaning of SPE columns (during preconditioning) and to maximize the removal of inorganic ions (in the final washing step). In brief, the pH of the azo dye solutions was adjusted to ~5 with 2 M sodium hydroxide and loaded onto 6 ml pre-conditioned SPE columns (Discovery® DSC-18 6 ML/500MG SPE, Sigma-Aldrich). The SPE columns were pre-conditioned by washing with 3 ml acetonitrile (HPLC grade,  $\geq 99.8\%$ , Thermo fisher Scientific) followed by 4 ml milli-Q  $\text{H}_2\text{O}$  (18.2 M $\Omega$ ). The SPE columns loaded with azo dye were then washed with 4 ml milli-Q  $\text{H}_2\text{O}$  and stored at  $-20$  °C for further analyses.

**Elution and analyses of HONO and  $\text{NO}_2^-$  azo dyes.** The frozen SPE columns were transported to the Terrestrial Ecosystem Research laboratory, University of Vienna, Austria, within one month after collection, where elution and analyses were performed. To avoid temperature effects (if any) during transportation, the frozen samples were transported in a sealed cooling box that contained ice bags. Immediately upon arrival, they were transferred to a  $-20$  °C freezer until elution. The elution and analyses of HONO and  $\text{NO}_2^-$  azo dyes were different from those in Wu et al.<sup>23</sup>. The fundamental difference was the instrument used to analyze the isotope ratios ( $^{15}\text{N}/^{14}\text{N}$ ) in HONO and  $\text{NO}_2^-$  azo dyes. In our study, we analyzed HONO and  $\text{NO}_2^-$  azo dyes with an UPLC system (Ultimate 3000, Thermo Fisher Scientific, Bremen, Germany) coupled to an Orbitrap Exactive HCD MS (Thermo Fisher Scientific) with a mass resolution of 50,000. The choice of the device was made to optimize the detection of the  $^{15}\text{N}$  signal in azo dyes, as suggested by Wu et al.<sup>23</sup>. The high resolution, high mass accuracy, and sensitivity of the Orbitrap-MS allowed us to separate the  $^{15}\text{N}$  and  $^{13}\text{C}$  isotopologue peaks that have a very small mass difference ( $\Delta_{\text{mass}}$  of 0.00632 Da)<sup>54,55</sup>. This and similar instruments are widely used to study metabolites, including those in soil extracts<sup>56</sup>. The choice of instrument (with electrospray ionization) eventually also led us to use eluents and reagents different from Wu et al.<sup>23</sup> for elution and chromatographic separation. Prior to elution, the SPE columns were transferred to room temperature for 20 minutes. Azo dyes were eluted with 5 ml eluent [80% methanol (HPLC grade, Sigma-Aldrich,  $\geq 99.9\%$ ) + 1% formic acid (98–100%, Merck Pro analysis)] using SPE vacuum manifolds. The eluates were diluted at 1:1 (v:v) ratio with milli-Q  $\text{H}_2\text{O}$  and analyzed on the same day of elution. More details are provided in the Supplementary Methods.

**Calculation of  $^{15}\text{N}$  enrichment in HONO and  $\text{NO}_2^-$  azo dyes.** The  $^{14}\text{N}$  and  $^{15}\text{N}$  peak areas in the samples and calibration standards were integrated manually with Xcalibur software and exported into Microsoft Excel sheets for further calculations. After blank correction of the  $^{14}\text{N}$  and  $^{15}\text{N}$  peaks of the samples and standards, we then calculated the concentrations ( $\mu\text{M}$ ) of the samples using the peak area sum (area of  $^{14}\text{N}$  plus area of  $^{15}\text{N}$  peaks), based on the slope and intercept build from the unlabeled concentration calibration standards using equation 1. Next, we calculated the percentage (%) of isotopically heavy (i.e.,  $^{15}\text{N}$ ) molecules of total molecules by dividing the peak area of the heavy isotopologues by the peak area sum of heavy and light isotopologues, as shown in Eq. 2. The atom%  $^{15}\text{N}$  of the azo dyes of HONO and  $\text{NO}_2^-$  were quantified from a series of polynomial functions generated from % of the heavy atoms (theoretical  $^{15}\text{N}$  in  $\text{NO}_2^-$  azo dye of isotope calibration standards) and atom%  $^{15}\text{N}$  measured in  $\text{NO}_2^-$  azo dyes by LCMS at two concentration levels of nitrite, 1.56  $\mu\text{M}$  and 25  $\mu\text{M}$ , and their average. These polynomial functions were applied depending upon the concentration and % of heavy isotopologues in the azo dye samples, which adapted within and between samples over time (e.g., LA vs. LNA vs. LNI treatments). The calibration curves for concentration from natural abundance calibration standards and theoretical  $^{15}\text{N}$  atom%  $^{15}\text{N}$  in  $\text{NO}_2^-$  azo dyes and atom%  $^{15}\text{N}$  as measured by LCMS at 1.56 and 25  $\mu\text{M}$  labeled calibration standards are shown in the Supplementary Methods and in Supplementary Figure 10.

$$\text{Azo dye concentration } (\mu\text{M}) = \frac{\text{peak area sum} - \text{intercept}}{\text{slope}} \quad (1)$$

$$\% \text{ of } ^{15}\text{N} \text{ atom} = \frac{\text{peak area of } ^{15}\text{N} \text{ atom}}{(^{14}\text{N} + ^{15}\text{N}) \text{ peak area}} \times 100 \quad (2)$$

**Gross rates.** Gross production and consumption rates of  $\text{NO}_2^-$ ,  $\text{NH}_4^+$ , and  $\text{NO}_3^-$  were calculated according to Kirkham and Batholomew<sup>53</sup>. More details are provided in the Supplementary Methods.



**Source contribution and determination of abiotic and biotic HONO fluxes.** The contributions (%) of  $\text{NH}_4^+$  oxidation,  $\text{NO}_3^-$  reduction, and organic nitrogen oxidation (the inset in Fig. 4) were calculated using the slopes (Fig. 2b–c) generated between  $^{15}\text{NO}_2^-$  and  $\text{HO}^{15}\text{NO}$  from the live soil samples of the LNi, LNa, and LA (only in the HOM soil) treatments. The contribution of  $\text{NH}_4^+$  oxidation and  $\text{NO}_3^-$  reduction was obtained by dividing the respective slopes by the slope between  $^{15}\text{NO}_2^-$  and  $\text{HO}^{15}\text{NO}$  in the LNi treatment. The contribution of organic N oxidation was obtained by subtracting the sum of  $\text{NH}_4^+$  oxidation and  $\text{NO}_3^-$  reduction from 100%. The contribution of a potentially unknown abiotic HONO source was quantified from the LNi treatment using Eqs. 3 and 4.

$$\text{atom}\%_{\text{mixture}} = (\text{atom}\%_{\text{source1}}) \times f_1 + (\text{atom}\%_{\text{source2}}) \times f_2 \quad (3)$$

$$f_1 = \frac{(\text{atom}\%_{\text{mixture}} - \text{atom}\%_{\text{source2}})}{(\text{atom}\%_{\text{source1}} - \text{atom}\%_{\text{source2}})} \quad (4)$$

In Eqs. 3 and 4, atom% represents the values of the mixture and the sources (i.e., source 1 and source 2), and the fractional contributions of source 1 and source 2 are represented by  $f_1$  and  $f_2$ , respectively. Here, the mixture was HONO, source 2 was  $\text{NO}_2^-$  and source 1 assumed to be at natural  $^{15}\text{N}$  abundance, i.e., 0.3663 atom %  $^{15}\text{N}$ . The fractional contribution of an unknown source (i.e.,  $f_1$ ) was determined using Eq. 4, with the assumption that the sum of fractional source contributions is 1, and that the contribution of  $\text{NO}_2^-$  ( $f_2$ ) is determined by  $1-f_1$ . The abiotic and biotic HONO emissions were quantified using the HONO emissions from live and sterile LNi treatment. To obtain an estimate of the abiotic HONO flux, we quantified the HONO flux, which solely originated from  $\text{NO}_2^-$  and was subtracted from the total HONO emitted there, in the LNi treatment that used fractional contributions of  $\text{NO}_2^-$  to HONO emissions ( $\text{ng N m}^{-2} \text{ s}^{-1}$ ) in the sterile soil samples. For the biotic HONO flux, HONO that originated from the  $\text{NO}_2^-$  added to the sterile soils was subtracted from the HONO measured from the live soil samples.

**Total HONO.** Total abiotic and biotic HONO represents the emission rates of soil HONO production averaged over 240 minutes of HONO flux measurements. To do that, first, total HONO in  $\text{ng N m}^{-2}$  was obtained for all replicates separately. Here, the HONO emission rates (in  $\mu\text{g N m}^{-2} \text{ s}^{-1}$ ) at each sampling point were multiplied by the time in seconds between the two consecutive sampling points, and their sum was calculated to obtain the total HONO. The total HONO ( $\text{ng N m}^{-2}$ ) thus obtained was divided by 14,400 ( $240 \times 60$ ) for all replicates separately to get the HONO emissions rate averaged over 240 minutes in  $\text{ng N m}^{-2} \text{ s}^{-1}$ . Finally, mean values and standard deviations were calculated for the abiotic (sterile soil samples) and biotic (live soil samples) sources.

**Soil analyses.** A detailed description of basic soil properties (Supplementary Table 1) and mineral N concentrations (Supplementary Figures 4–5) are provided in the Supplementary Methods.

**Nucleic acid extractions, purification, and gene quantification.** Nucleic acids in both soils were extracted from the control samples, which were used for HONO flux measurements in accordance with a protocol based on Yeates and Gillings<sup>57</sup> and Griffiths et al.<sup>58</sup>. Real time quantitative polymerase chain reactions were used for gene quantification. Details on nucleic acid extractions and gene quantification are explained in the Supplementary Methods and in Supplementary Tables 5–6.

**Statistics.** Statistical analysis and graphical presentations were performed in R statistical software (R version 3.6.1), unless otherwise specified. Before performing a statistical test, the distribution of the data was assessed using the Shapiro–Wilk test, Q–Q plots, and histograms, and were transformed (log or square root) when required. More details are provided in the Supplementary Methods.

## Data availability

All data produced in this study are available at <https://doi.org/10.5281/zenodo.4503384>.

Received: 3 September 2020; Accepted: 9 February 2021;

Published online: 05 March 2021

## References

- Elshorbany, Y. F. et al. Summertime photochemical ozone formation in Santiago, Chile. *Atmos. Environ.* **43**, 6398–6407 (2009).
- Lelieveld, J., Dentener, F. J., Peters, W. & Krol, M. C. On the role of hydroxyl radicals in the self-cleansing capacity of the troposphere. *Atmos. Chem. Phys.* **4**, 2337–2344 (2004).
- Riedel, K. & Lassey, K. Detergent of the atmosphere. *Water Atmos.* **16** (2008).
- Peters, M. D. et al. Chemical aging and the hydrophobic-to-hydrophilic conversion of carbonaceous aerosol. *Geophys. Res. Lett.* **33**, L24806 (2006).
- Claeys, M. Formation of secondary organic aerosols through photooxidation of isoprene. *Science* **303**, 1173–1176 (2004).
- Kleffmann, J. Daytime formation of nitrous acid: a major source of OH radicals in a forest. *Geophys. Res. Lett.* **32**, L05818 (2005).
- Acker, K. et al. Strong daytime production of OH from  $\text{HNO}_2$  at a rural mountain site. *Geophys. Res. Lett.* **33**, L02809 (2006).
- Su, H. et al. Nitrous acid (HONO) and its daytime sources at a rural site during the 2004 PRIDE-PRD experiment in China. *J. Geophys. Res.* **113**, D14312 (2008).
- Su, H. et al. Soil nitrite as a source of atmospheric HONO and OH radicals. *Science* **333**, 1616–1618 (2011).
- Oswald, R. et al. HONO Emissions from soil bacteria as a major source of atmospheric reactive nitrogen. *Science* **341**, 1233–1235 (2013).
- Scharko, N. K. et al. Combined flux chamber and genomics approach links nitrous acid emissions to ammonia oxidizing bacteria and archaea in urban and agricultural soil. *Environ. Sci. Technol.* **49**, 13825–13834 (2015).
- Maljanen, M., Yli-Pirilä, P., Hytönen, J., Joutsensaari, J. & Martikainen, P. J. Acidic northern soils as sources of atmospheric nitrous acid (HONO). *Soil Biol. Biochem.* **67**, 94–97 (2013).
- Bhattarai, H. R., Virkajärvi, P., Yli-Pirilä, P. & Maljanen, M. Emissions of atmospherically important nitrous acid (HONO) gas from northern grassland soil increases in the presence of nitrite ( $\text{NO}_2^-$ ). *Agric. Ecosyst. Environ.* **256**, 194–199 (2018).
- Tang, K. et al. A dual dynamic chamber system based on IBBCEAS for measuring fluxes of nitrous acid in agricultural fields in the North China Plain. *Atmos. Environ.* **196**, 10–19 (2019).
- Bhattarai, H. R. et al. Germinating wheat promotes the emission of atmospherically significant nitrous acid (HONO) gas from soils. *Soil Biol. Biochem.* **136**, 107518 (2019).
- Ramsay, R. et al. Surface–atmosphere exchange of inorganic water-soluble gases and associated ions in bulk aerosol above agricultural grassland pre- and postfertilisation. *Atmos. Chem. Phys.* **18**, 16953–16978 (2018).
- Mushinski, R. M. et al. Microbial mechanisms and ecosystem flux estimation for aerobic  $\text{NO}_y$  emissions from deciduous forest soils. *Proc. Natl Acad. Sci. USA* **116**, 2138–2145 (2019).
- Cole, J. A. & Brown, C. M. Nitrite reduction to ammonia by fermentative bacteria: a short circuit in the biological nitrogen cycle. *FEMS Microbiol. Lett.* **7**, 65–72 (1980).
- Knowles, R. Denitrification. *Microbiol. Rev.* **46**, 43–70 (1982).
- Papen, H., von Berg, R., Hinkel, I., Thoene, B. & Rennenberg, H. Heterotrophic nitrification by *Alcaligenes faecalis*:  $\text{NO}_2^-$ ,  $\text{NO}_3^-$ ,  $\text{N}_2\text{O}$ , and  $\text{NO}$  production in exponentially growing cultures. *Appl. Environ. Microbiol.* **55**, 2068–2072 (1989).
- Ermel, M. et al. Hydroxylamine released by nitrifying microorganisms is a precursor for HONO emission from drying soils. *Sci. Rep.* **8**, 1877 (2018).
- Kubota, M. & Asami, T. Source of nitrous acid volatilized from upland soils. *Soil Sci. Plant Nutr.* **31**, 35–42 (1985).
- Wu, D. et al. Novel tracer method to measure isotopic labeled gas-phase nitrous acid ( $\text{HO}^{15}\text{NO}$ ) in biogeochemical studies. *Environ. Sci. Technol.* **48**, 8021–8027 (2014).
- Gamble, T. N., Betlach, M. R. & Tiedje, J. M. Numerically dominant denitrifying bacteria from world soils. *Appl. Environ. Microbiol.* **33**, 926–939 (1977).
- Wu, D. et al. Soil HONO emissions at high moisture content are driven by microbial nitrate reduction to nitrite: tackling the HONO puzzle. *ISME J* **13**, 1688–1699 (2019).
- Sextstone, A. J., Revsbech, N. P., Parkin, T. B. & Tiedje, J. M. Direct measurement of oxygen profiles and denitrification rates in soil aggregates. *Soil Sci. Soc. Am. J.* **49**, 645–651 (1985).
- Stevens, R. J. & Laughlin, R. J. Measurement of nitrous oxide and di-nitrogen emissions from agricultural soils. *Nutr. Cycl. Agroecosyst.* **52**, 131–139 (1998).
- Bremner, J. M. & Shaw, K. Denitrification in soil. II. Factors affecting denitrification. *J. Agric. Sci.* **51**, 40–52 (1958).
- Sahrawat, K. L. Factors affecting nitrification in soils. *Commun. Soil Sci. Plant Anal.* **39**, 1436–1446 (2008).
- Kulmala, M. & Petaja, T. Soil nitrites influence atmospheric chemistry. *Science* **333**, 1586–1587 (2011).
- Liu, Y. et al. A Comprehensive model test of the HONO sources constrained to field measurements at rural north china plain. *Environ. Sci. Technol.* **53**, 3517–3525 (2019).
- Food and Agriculture Organization of the United Nations. *FAO statistical yearbook 2013*. (Food & Agriculture Organi, 2013).
- Ritchie, H. & Roser, M. *Crop Yields*. Published online at OurWorldInData.org. Retrieved from: <https://ourworldindata.org/crop-yields> (2013).
- Tilman, D. Forecasting agriculturally driven global environmental change. *Science* **292**, 281–284 (2001).

35. Berns, A. E. et al. Effect of gamma-sterilization and autoclaving on soil organic matter structure as studied by solid state NMR, UV and fluorescence spectroscopy. *Eur. J. Soil Sci.* **59**, 540–550 (2008).
36. Fry, B. *Stable isotope ecology*. 139–142 (Springer, 2008).
37. Weber, B. et al. Biological soil crusts accelerate the nitrogen cycle through large NO and HONO emissions in drylands. *Proc. Natl Acad. Sci.* **112**, 15384–15389 (2015).
38. Philippot, L. Tracking nitrate reducers and denitrifiers in the environment. *Biochem. Soc. Transact.* **33**, 200–204 (2005).
39. Mohan, S. B., Schmid, M., Jetten, M. & Cole, J. Detection and widespread distribution of the *nrfA* gene encoding nitrite reduction to ammonia, a short circuit in the biological nitrogen cycle that competes with denitrification. *FEMS Microbiol. Ecol.* **49**, 433–443 (2004).
40. Davidson, E. A., Chorover, J. & Dail, D. B. A mechanism of abiotic immobilization of nitrate in forest ecosystems: the ferrous wheel hypothesis. *Glob. Change Biol.* **9**, 228–236 (2003).
41. Nicol, G. W., Leininger, S., Schleper, C. & Prosser, J. I. The influence of soil pH on the diversity, abundance and transcriptional activity of ammonia oxidizing archaea and bacteria. *Environ. Microbiol.* **10**, 2966–2978 (2008).
42. Prosser, J. I. & Nicol, G. W. Archaeal and bacterial ammonia-oxidisers in soil: the quest for niche specialisation and differentiation. *Trends Microbiol.* **20**, 523–531 (2012).
43. Zumft, W. G. Cell biology and molecular basis of denitrification. *Microbiol. Mol. Biol. Rev.* **61**, 533–616 (1997).
44. Finlayson-Pitts, B. J., Wingen, L. M., Sumner, A. L., Syomin, D. & Ramazan, K. A. The heterogeneous hydrolysis of NO<sub>2</sub> in laboratory systems and in outdoor and indoor atmospheres: an integrated mechanism. *Phys. Chem. Chem. Phys.* **5**, 223–242 (2003).
45. Stemmler, K., Ammann, M., Donders, C., Kleffmann, J. & George, C. Photosensitized reduction of nitrogen dioxide on humic acid as a source of nitrous acid. *Nature* **440**, 195–198 (2006).
46. Cleemput, O. & Samater, A. H. Nitrite in soils: accumulation and role in the formation of gaseous N compounds. *Fertil. Res.* **45**, 81–89 (1995).
47. Chalk, P. M. & Smith, C. J. Chemodenitrification. in *Gaseous Loss of Nitrogen from Plant-Soil Systems* (eds. Freney, J. R. & Simpson, J. R.) 65–89 (Springer Netherlands, 1983).
48. Medinets, S., Skiba, U., Rennenberg, H. & Butterbach-Bahl, K. A review of soil NO transformation: associated processes and possible physiological significance on organisms. *Soil Biol. Biochem.* **80**, 92–117 (2015).
49. Wei, J. et al. N<sub>2</sub>O and NO<sub>x</sub> emissions by reactions of nitrite with soil organic matter of a Norway spruce forest. *Biogeochemistry* **132**, 325–342 (2017).
50. Liu, Y. et al. Semi-quantitative understanding of source contribution to nitrous acid (HONO) based on 1 year of continuous observation at the SORPES station in eastern China. *Atmos. Chem. Phys.* **19**, 13289–13308 (2019).
51. FAO. World reference base for soil resources 2014: international soil classification system for naming soils and creating legends for soil maps. (FAO, 2014).
52. Kleffmann, J., Heland, J., Kurtenbach, R., Lörzer, J. & Wiesen, P. A new instrument (LOPAP) for the detection of nitrous acid (HONO). *Environ. Sci. Pollut. Res.* **9**, 48–54 (2002).
53. Kirkham, D. & Bartholomew, W. V. Equations for following nutrient transformations in soil, utilizing tracer data. *Soil Sci. Soc. Am. J.* **18**, 33 (1954).
54. Lu, W. et al. Metabolomic analysis via reversed-phase ion-pairing liquid chromatography coupled to a stand alone orbitrap mass spectrometer. *Anal. Chem.* **82**, 3212–3221 (2010).
55. You, L., Zhang, B. & Tang, Y. Application of stable isotope-assisted metabolomics for cell metabolism studies. *Metabolites* **4**, 142–165 (2014).
56. Hu, Y., Zheng, Q. & Wanek, W. Flux analysis of free amino sugars and amino acids in soils by isotope tracing with a novel liquid chromatography/high resolution mass spectrometry platform. *Anal. Chem.* **89**, 9192–9200 (2017).
57. Yeates, C. & Gillings, M. Rapid purification of DNA from soil for molecular biodiversity analysis. *Lett. Appl. Microbiol.* **27**, 49–53 (1998).
58. Griffiths, R. I., Whiteley, A. S., O'Donnell, A. G. & Bailey, M. J. Rapid method for coextraction of DNA and RNA from natural environments for analysis of ribosomal DNA- and rRNA-based microbial community composition. *Appl. Environ. Microbiol.* **66**, 5488–5491 (2000).

### Acknowledgements

This study was funded by the Academy of Finland under the project “The origin of nitrous acid (HONO) emissions from northern soils and linkages to nitrogen cycle processes” (grant no. 297735) and the doctoral program of the University of Eastern Finland (grant to H. R. Bhattarai). We also thank the Academy of Finland Center of Excellence program (project no. 307331) for supporting this study. We thank Jaana Rissanen for laboratory assistance and Pasi Yli-Pirilä for technical assistance. We highly appreciate all the laboratory and technical personnel for their help during our research visit in the Terrestrial Ecosystem Research laboratory at the University of Vienna. We also thank Natural Resources Institute Finland (LUKE) for providing the study sites and for providing data on soil texture.

### Author contributions

H.R.B., W.W., C.B., M.L., H.N. and M.M. designed the experiments. <sup>15</sup>N analyses of HONO and NO<sub>2</sub><sup>-</sup> were performed by H.R.B., M.L., Y.H. and W.W., H.R.B. and C.B. analyzed the acid traps for <sup>15</sup>NO<sub>3</sub><sup>-</sup> and <sup>15</sup>NH<sub>4</sub><sup>+</sup>. H.R.B. measured the HONO flux. H.R.B., M.L. and M.M. analyzed the soil physicochemical properties. J.R. and H.S. did the quantification of functional genes. H.R.B. processed all the data and did the statistical tests and wrote the first draft of the manuscript. W.W. produced the synthesis data on global HONO flux rates and gross nitrite production rates from soils and contributed equally to the writing of the manuscript. All authors contributed, read, and approved the manuscript.

### Competing interests

The authors declare no competing interests.

### Additional information


**Supplementary information** The online version contains supplementary material available at <https://doi.org/10.1038/s43247-021-00125-7>.

**Correspondence** and requests for materials should be addressed to H.R.B.

**Peer review information** Primary handling editors: Leiyl Chen, Joe Aslin, Clare Davis.

**Reprints and permission information** is available at <http://www.nature.com/reprints>

**Publisher's note** Springer Nature remains neutral with regard to jurisdictional claims in published maps and institutional affiliations.

 **Open Access** This article is licensed under a Creative Commons Attribution 4.0 International License, which permits use, sharing, adaptation, distribution and reproduction in any medium or format, as long as you give appropriate credit to the original author(s) and the source, provide a link to the Creative Commons license, and indicate if changes were made. The images or other third party material in this article are included in the article's Creative Commons license, unless indicated otherwise in a credit line to the material. If material is not included in the article's Creative Commons license and your intended use is not permitted by statutory regulation or exceeds the permitted use, you will need to obtain permission directly from the copyright holder. To view a copy of this license, visit <http://creativecommons.org/licenses/by/4.0/>.

© The Author(s) 2021